Surface and Interfacial FTIR Spectroscopic Studies of Latexes. XII. Particle Size Effect and Surfactant Behavior in Electrodeposited Sty/*n*-BA Latex Films

B.-J. NIU and MAREK W. URBAN*

Department of Polymers and Coatings, North Dakota State University, Fargo, North Dakota 58105

SYNOPSIS

Polarized attenuated total reflection Fourier transform infrared spectroscopy was used to assess the mobility and orientation of sodium dioctylsulfosuccinate surfactant molecules at the film–air (F–A) and film–substrate (F–S) interfaces in electrodeposited latex films. Copolymer compositions ranging from 100% poly(*n*-BA) to 50%/50% Sty/*n*-BA were examined. When particle diameters are 50 and 100 nm, it appears that the 1046 cm^{-1} band is detected at the F–A and F–S interfaces. However, the 1056 cm^{-1} band is detected only for 50%/50% Sty/*n*-BA at the F–A interface with an average particle diameter of 100 nm. These studies allow us to determine that at the F–A interface, SDOSS surfactant molecules are preferentially parallel to the surface. Utilizing electrodeposition of latex particles, it is possible to slow the coalescence process, which ultimately allows us to follow diffusion and mobility of low-molecular-weight SDOSS surfactant molecules. © 1996 John Wiley & Sons, Inc.

INTRODUCTION

Our previous studies[1-8] indicated that the mobility of low-molecular-weight materials, in particular surfactant molecules, is influenced by the glass transition temperature (T_g), and subsequently by the free volume of a polymer matrix, surface tension at the film–air (F–A) and film–substrate (F–S) interfaces, compatibility, and coalescence times. The evaporation rate of water is also an important factor since it affects latex coalescence and film formation.[9,10] In an effort to understand how extended coalescence times may affect surfactant mobility after latex coalescence, a new concept of depositing latex films will be introduced in this study; namely, latex electrodeposition. Although this approach is borrowed from the commonly used electrodeposition of water-borne polymers, the concept may be beneficial in latexes not only as an efficient method of depositing films but also as one way to slow the coalescence process.

When an aqueous dispersion of latex particles is deposited on a substrate, it takes a relatively long time for such a film to coalesce. When the same latex particles are electrodeposited, they bombard a metallic substrate and become affixed to it. Although this process leads to waterless particles deposited on a substrate, a lack of water molecules in the interstices leads to a rough film. In this study, we focus on how particle size and various latex compositions influence surfactant mobility and their orientations near the F–A and F–S interfaces in electrodeposited latex films.

Like the previous studies, this one uses polarized attenuated total reflection Fourier transform infrared (ATR FTIR) spectroscopy, with recently developed algorithm for spectral analysis,[11,12] to monitor the content of surfactant molecules and the orientation of $SO_3^-Na^+$ hydrophilic end groups on surfactant molecules at the F–A and F–S interfaces.

EXPERIMENTAL

Latex Preparation

The latex copolymer compositions 100% *n*-butyl acrylate (*n*-BA) and 10%/90%, 20%/80%, 30%/70%,

* To whom correspondence should be addressed.

Journal of Applied Polymer Science, Vol. 60, 379–387 (1996)
 CCC 0021-8995/96/030379-09

40%/60%, and 50%/50% styrene/*n*-BA (Sty/*n*-BA) were synthesized by a semicontinuous emulsion polymerization process which was described in the previous publication.[1]

Electrodeposition

100% *n*-BA and 10%/90%, 20%/80%, 30%/70%, 40%/60%, and 50%/50% Sty/*n*-BA latex copolymers with two different average particle diameters, 50 and 100 nm, were electrodeposited for 3 min on an aluminum plate (25 mm × 100 mm), using a DC power supply (Dreser Electric Co.) set at 30 V. Such coalesced latex films, with an approximate thickness of 250 μm, were placed into a glove box and allowed to coalesce from 1 to 6 h at 80% relative humidity and 22°C.

Spectroscopic Analysis

Polarized ATR FTIR spectroscopy was used to analyze F–A and F–S interfaces of latex films. All ATR FTIR spectra were recorded on a Digilab FTS-20 instrument, equipped with a rectangular ATR attachment (Spectra Tech) containing KRS-5 crystal aligned to give an incident beam angle of 45 degrees. In a typical experiment, 200 scans were collected at a resolution of 4 cm^{-1} with transverse magnetic (TM) (0°) and transverse electric (TE) (90°) polarization filters. All spectra were transferred to a PC-compatible computer for further spectra analysis utilizing Spectra Calc software (Galactic, Inc.). The spectra were corrected for optical effects using a Q-ATR algorithm.[11,12]

RESULTS AND DISCUSSION

Although it would be appropriate to begin the discussion of electrodeposited latex films by comparing the electrodeposited latex results with the data on latex films deposited by traditional means, the time scales for coalescence in these two procedures are so different that such a comparison would have no meaning. It appears that obtaining solid film by conventional deposition would take about 48 h, whereas the electrodeposition time scale is shortened to approximately 30 min.

Let us begin this analysis with the description of a 50%/50% Sty/*n*-BA copolymer. ATR FTIR spectra of 50%/50% Sty/*n*-BA electrodeposited copolymer latex films with a particle size of 50 nm allowed to coalesce from 1 to 6 h are shown in Figure 1, traces (A) to (F), respectively. The spectra were

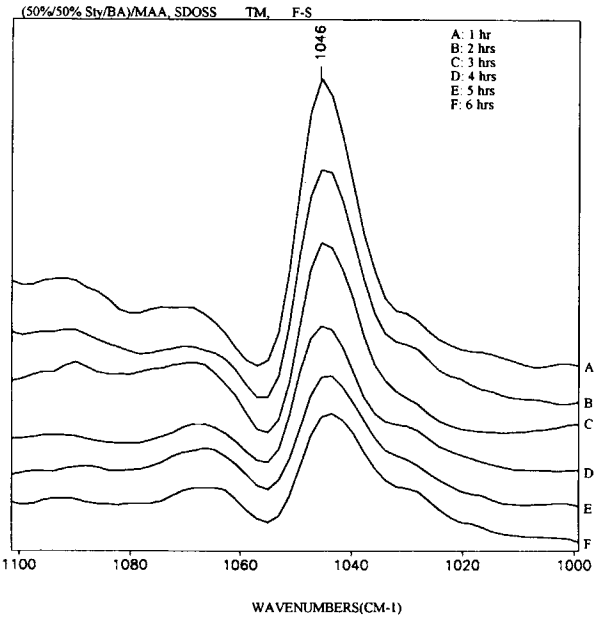

Figure 1 ATR FTIR spectra of 50%/50% Sty/*n*-BA latex copolymer with a particle size of 50 nm recorded from the F–S interface with TM polarization. Coalescence time: (A) 1 h; (B) 2 h; (C) 3 h; (D) 4 h; (E) 5 h; (F) 6 h.

recorded from the F–S interface using TM polarization. It appears that the intensity of the 1046 cm^{-1} band normalized to the 841 cm^{-1} band decreases at extended coalescence times. Because the 1046 cm^{-1} band is attributed to the S—O symmetric stretching modes of $SO_3^- Na^+$ groups associated with H_2O, the detected changes suggest that H_2O molecules migrate from the interior of the latex film to the surface, where they become associated with the $SO_3^- Na^+$ hydrophilic groups of sodium dioctylsulfosuccinate (SDOSS). Although the magnitude of this process is different near the F–A interface, diminishing intensity of the 1046 cm^{-1} band (not shown) can be detected. Regardless of the kinetics of the process occurring at the F–A and F–S interfaces, the strongest intensity of the 1046 cm^{-1} band at the F–A interface is detected 1 h after coalescence. In an effort to compare how the intensity at the 1046 cm^{-1} changes at the F–A and F–S interfaces, Figure 2 was constructed, to illustrate the 1046 cm^{-1} band intensity changes plotted as functions of the coalescence time. Curve (A) of Figure 2 shows the 1046 cm^{-1} intensity changes at the F–A interface; curve B was obtained from the F–S interface.

With these data in mind let us address two issues that appear to be important in the context of these as well as our previous studies.[1-9] First, the band at 1056 cm^{-1}, which is due to the S—O stretching band resulting from $SO_3^- Na^+ \cdots HOOC$ associations,[2-9]

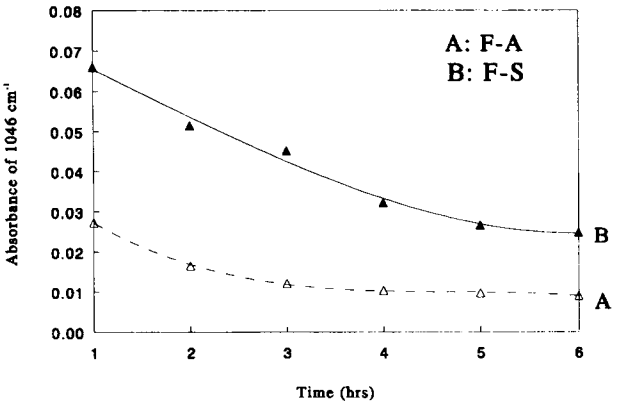

Figure 2 Plot of absorbance of the 1046 cm^{-1} band as a function of coalescence time: (A) F–A interface; (B) F–S interface.

is not detected. Furthermore, as illustrated in Figure 2, the 1046 cm^{-1} band decreases at both interfaces with extended coalescence times.

In order to assess the origin of these changes, let us realize that for the same latex, but with an average particle size of 100 nm, the situation is quite different. As illustrated in Figure 3, traces (A)–(F), which show a series of the ATR FTIR spectra recorded from the F–A interface using TE polarization with a particle size of 100 nm, both 1056 and 1046 cm^{-1} bands are detected. As shown in Figure 3, trace (F), this is mostly pronounced for the 50%/50% Sty/*n*-BA copolymer specimen. In an effort to establish the origin of the differences between 50- and 100-nm latex particles, let us now realize that a larger latex particle size is accomplished by slower stirring of the reaction mixture during latex polymerization. Under such circumstances, the reactivity ratios of the starting monomers will have the dominating effect on the latex particle composition. As we have already established and cross-referenced with the literature data,[9] a comparison of the reactivity ratios for styrene and *n*-BA favors styrene homopolymerization, and the formation of the polystyrene core and poly(*n*-BA) shell occurs for the larger particle sizes.[13] In contrast, for smaller particle sizes, more homogeneous distribution for Sty/*n*-BA particle cross-section is anticipated. As a result, the 1056 cm^{-1} band is detected for larger particle-size latexes, but it is not detectable for smaller particles since there are minimal or no $COOH \cdots SO_3^- Na^+$ interactions. Therefore, only the 1046 cm^{-1} band is detected. In view of the above considerations and the results for 50%/50% polySty and poly(*n*-BA) mixed latexes, the results for 50- and 100-nm-diameter copolymers suggest that there are regions near the surface which contain COOH groups of poly(*n*-BA), facilitating $SO_3^- Na^+$ hydrophilic group interactions.

One issue that should be addressed at this point is that all presented spectra were obtained using polarized light. Therefore, band intensities of vibrations with the dipole moment changes aligned in the direction of the electric vector of polarization will be enhanced. If this is not the case, the band intensities will remain the same regardless of polarization. With this in mind, let us examine the latex data for a 50-nm-diameter particle, presented in Figure 2, and realize that the 1046 cm^{-1} band does not exhibit intensity changes with polarization changes. Therefore, no preferential orientation of the $SO_3^- Na^+$ groups exists. In contrast, the data for 100-nm-diameter latex particles indicate that by changing polarization from TE (Fig. 3) to TM (Fig. 4), relative intensities of the 1046 and 1056 cm^{-1} bands change, indicating that the $SO_3^- Na^+$ groups exhibit preferential orientation. Although at this point one could attempt to depict a scenario for the orientation of $SO_3^- Na^+$ groups of SDOSS, let us temporarily postpone that analysis and discuss how the particle size will influence SDOSS mobility.

Although it may seem that the latex particle size has nothing to do with the diffusion of surfactant

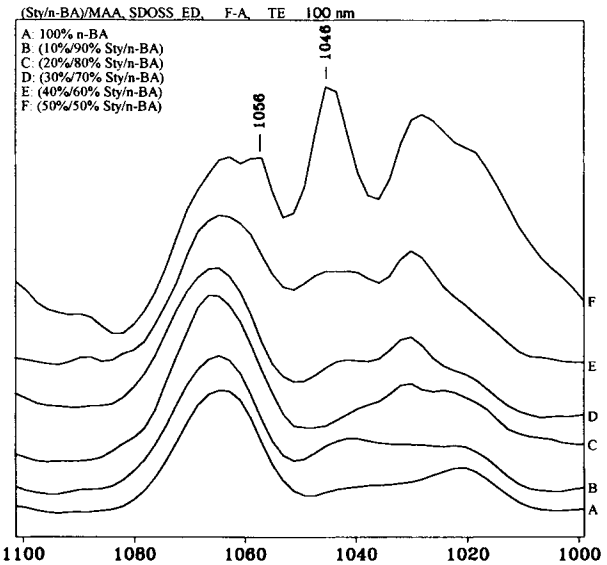

Figure 3 ATR FTIR spectra in the S—O symmetric stretching region of Sty/*n*-BA latex copolymers with a particle size of 100 nm recorded from the F–A interface with TE polarization: (A) 100% *n*-BA; (B) 10%/90% Sty/*n*-BA; (C) 20%/80% Sty/*n*-BA; (D) 30%/70% Sty/*n*-BA; (E) 40%/60% Sty/*n*-BA; (F) 50%/50% Sty/*n*-BA. (Coalescence time: 6 h).

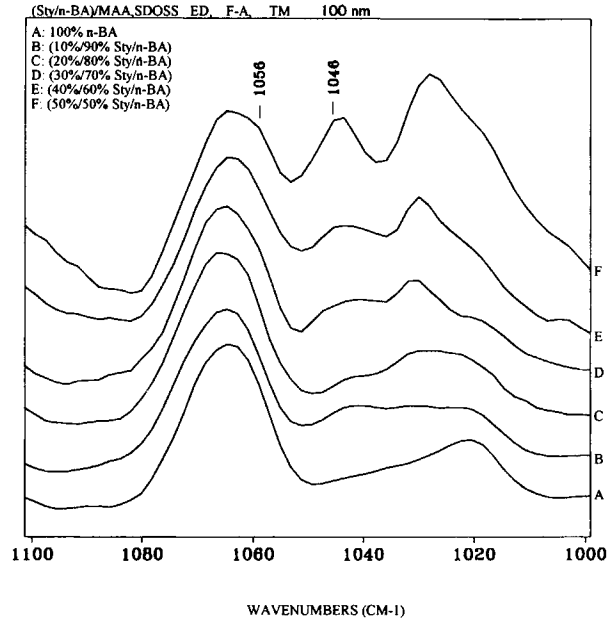

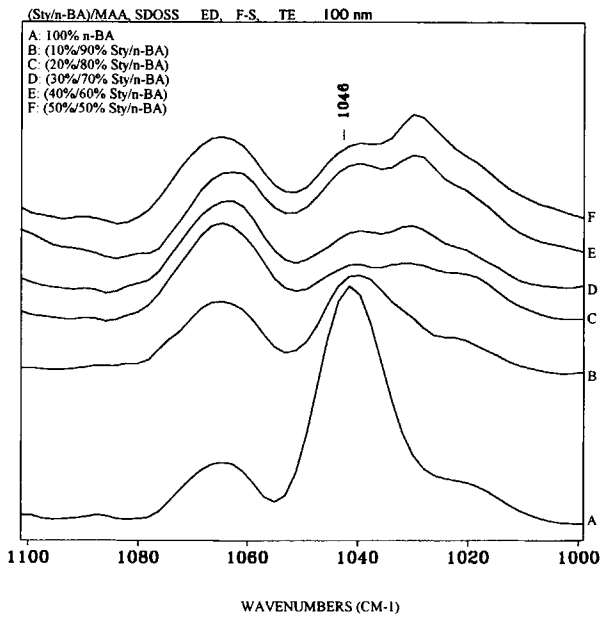

Figure 4 ATR FTIR spectra in the S—O symmetric stretching region of Sty/*n*-BA latex copolymers with a particle size of 100 nm recorded from the F–A interface with TM polarization: (A) 100% *n*-BA; (B) 10%/90% Sty/*n*-BA; (C) 20%/80% Sty/*n*-BA; (D) 30%/70% Sty/*n*-BA; (E) 40%/60% Sty/*n*-BA; (F) 50%/50% Sty/*n*-BA. (Coalescence time: 6 h).

molecules in coalesced films, let us compare a series of the ATR spectra recorded from the F–S interface of latex compositions that are identical but have different particle sizes. A comparison of the spectra for 50- and 100-nm-diameter-particle latexes, shown in Figures 5(a) and (b), indicates that for a 100% *n*-BA latex composition, the band at 1046 cm^{-1} is the strongest when the latex particle size is 100 nm. In contrast, for a 50-nm-particle-size latex, the 1046 cm^{-1} band is the strongest for a 50%/50% Sty/*n*-BA.

At this point let us review our primary motivation for electrodepositing latex films on a metal substrate: the concept is to bombard the substrate with latex particles and therefore slow their coalescence by minimizing the amount of water in particle interstices. If we now realize the experimental conditions prior to electrodeposition, the results illustrated in Figures 5(a) and (b) become understandable. When electric potential is applied to a latex aqueous suspension, charged particles will become mobilized. In the case of Sty/*n*-BA latex, the latex particles are stabilized by ionic SDOSS surfactant molecules. However, there are also free SDOSS molecules dispersed in H_2O; due to their inherently lower mass and volume, these species will travel faster. Because

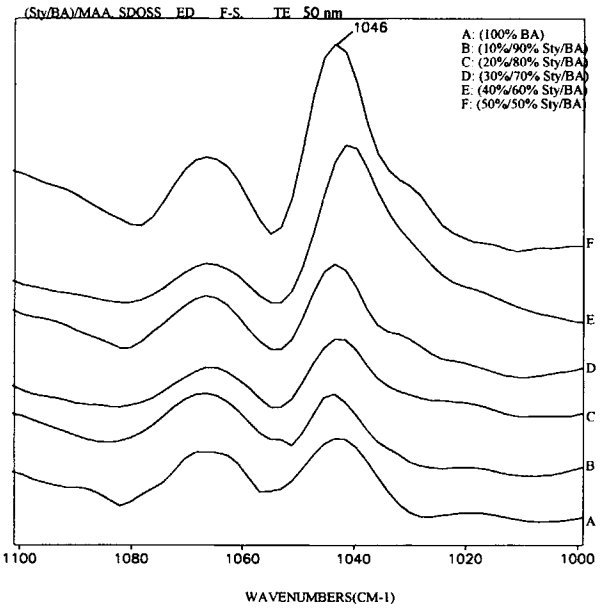

Figure 5 (a) ATR FTIR spectra in the S—O symmetric stretching region of Sty/*n*-BA latex copolymers with a particle size of 100 nm recorded from the F–S interface with TE polarization: (A) 100% *n*-BA; (B) 10%/90% Sty/*n*-BA; (C) 20%/80% Sty/*n*-BA; (D) 30%/70% Sty/*n*-BA; (E) 40%/60% Sty/*n*-BA; (F) 50%/50% Sty/*n*-BA. (Coalescence time: 6 h). (b) ATR FTIR spectra in the S—O symmetric stretching region of Sty/*n*-BA latex copolymers with a particle size of 50 nm recorded from the F–S interface with TE polarization: (A) 100% *n*-BA; (B) 10%/90% Sty/*n*-BA; (C) 20%/80% Sty/*n*-BA; (D) 30%/70% Sty/*n*-BA; (E) 40%/60% Sty/*n*-BA; (F) 50%/50% Sty/*n*-BA. (Coalescence time: 6 h).

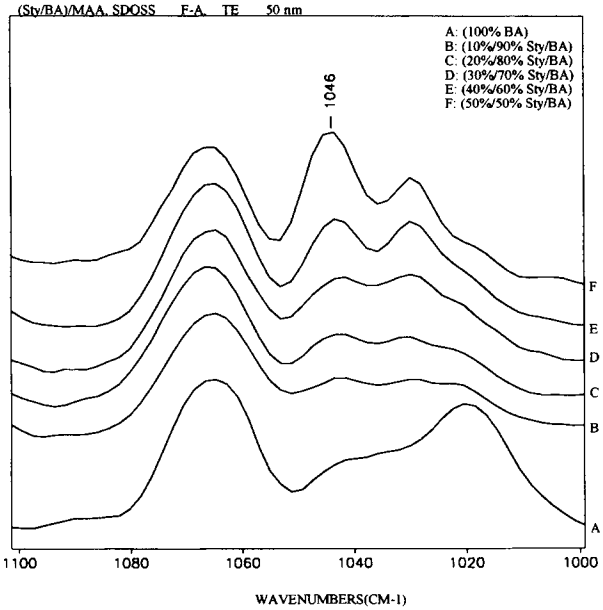

Figure 6 ATR FTIR spectra in the S—O symmetric stretching region of Sty/*n*-BA latex copolymers with a particle size of 50 nm recorded from the F–A interface with TE polarization: (A) 100% *n*-BA; (B) 10%/90% Sty/*n*-BA; (C) 20%/80% Sty/*n*-BA; (D) 30%/70% Sty/*n*-BA; (E) 40%/60% Sty/*n*-BA; (F) 50%/50% Sty/*n*-BA. (Coalescence time: 6 h).

in this experimental setup the anode is a positively charged substrate, anionic $SO_3^-Na^+$ groups will be deposited first. Therefore, initially more surfactant molecules arrive at the F–S interface, and this is why SDOSS is detected for the specimens allowed to coalescence for 1 h. However, SDOSS molecules have no chance to associate with COOH latex groups, which would ultimately lead to the presence of the 1056 cm^{-1} band. This band is not detected for a 50%/50% Sty/*n*-BA composition with particle sizes of 50 and 100 nm. At extended coalescence times, the remaining water evaporates and fewer associations exist between SDOSS molecules and H_2O. As illustrated in Figure 1, traces (A)-(F), this results in a decrease at the 1046 cm^{-1} band.

One property of surfactant molecules is their tendency to migrate to areas where there is an excess of surface energy, in an attempt to compensate for the interfacial surface tension. While interfacial surface tension is one source for mobility of surfactant molecules, a driving force in the opposite direction is water evaporation out of the film, which leads to the migration of SDOSS molecules to the F–A interface. This results in diffusion of SDOSS molecules toward the surface. In view of the above considerations, and because the T_g of a latex is inherently related to its free volume,[14-16] we varied the latex composition in order to identify how excess of the free volume will influence surfactant mobility in electrodeposited latex films. Figure 5(b), traces (A)-(F), illustrate ATR FTIR spectra of 100% *n*-BA and 10%/90%, 20%/80%, 30%/70%, 40%/60%, and 50%/50% Sty/*n*-BA of latex films at the F–S interface recorded with TE polarization. The figure shows that the 1046 cm^{-1} band intensity increases with higher styrene content, but no detectable difference in the band intensity changes was observed between TE and TM (not shown) polarizations. These observations indicate that the surfactant molecules exhibit no preferential orientation at the F–S interface. For a higher styrene content, however, T_g of the latex increases,[10] and compatibility between ionic surfactant molecules and the latex copolymer is not favorable. Since the presence of styrene introduces more hydrophobicity to latex particles, surfactant molecules are likely to be pushed out of the styrene phase, and an excess of non-associated surfactants exists in the aqueous phase. Therefore, they migrate toward a metallic substrate because of the electric potential difference between the electrodes, and more surfactant molecules are detected for a 50%/50% Sty/*n*-BA composition at the F–S interface. On the other hand, only a few surfactant molecules are detected for a 100% *n*-BA latex composition.

These observations, along with a lack of the 1056 cm^{-1} band, indicate that particle size has a significant effect on the H-bonding between $SO_3^-Na^+$ and COOH groups. Figure 6, traces (A)-(F), show ATR FTIR spectra of 100% *n*-BA and 10%/90%, 20%/80%, 30%/70%, 40%/60%, and 50%/50% Sty/*n*-BA latex films at the F–A interface, recorded with TE polarization. It appears that, like the F–A interface, excessive amounts of surfactant molecules are detected for a 50%/50% Sty/*n*-BA latex composition. Furthermore, the amount of SDOSS is highest for 50%/50% Sty/*n*-BA at the F–S interface. This behavior is attributed to the fact that a lower free volume is anticipated for higher-T_g copolymers, thus inhibiting water and surfactant molecules from diffusing out of the F–S interface. On the other hand, the F–A interface is exposed to air, thus facilitating a diffusion of water out of the film.

Let us now concentrate on the S—O asymmetric stretching region and compare the spectra recorded from the F–A interface for various Sty/*n*-BA compositions. As we recall,[2] the band at 1216 cm^{-1} attributed to the S—O asymmetric stretching vibrational modes of $SO_3^-Na^+$ end groups on SDOSS molecules split to two bands at 1261 and 1209 cm^{-1}

due to H-bonding associations between SDOSS molecules with COOH groups and H_2O, respectively. Due to the same interactions, the 1241 cm^{-1} band attributed to the C—O—C asymmetric stretching vibrational modes for hydrophobic ends on SDOSS molecules also split to two bands, at 1290 and 1236 cm^{-1}. Figure 7, traces (A)–(F), illustrate ATR FTIR spectra of 100% *n*-BA and 10%/90%, 20%/80%, 30%/70%, 40%/60%, and 50%/50% Sty/*n*-BA latex films at the F–A interface, recorded with TE polarization. It appears that only in the 50%/50% Sty/*n*–BA composition are the bands at 1261 and 1209 cm^{-1} detected [trace (F)]. In contrast, the results presented in Figure 8, traces (A)–(F), show that these bands are not detected at the F–A interface spectra recorded in TM polarization. Instead, the bands at 1290 and 1236 cm^{-1} are detected for 50%/50% Sty/*n*-BA composition [trace (F)]. These observations indicate that the hydrophilic $SO_3^-Na^+$ end groups on SDOSS molecules are preferentially parallel to the surface, and that the enhancement of the 1290 and 1236 cm^{-1} bands recorded with TM polarization from the F–A interface [Fig. 8, trace (F)] results from the fact that the hydrophobic end groups of SDOSS molecules are preferentially perpendicular to the F–A interface.

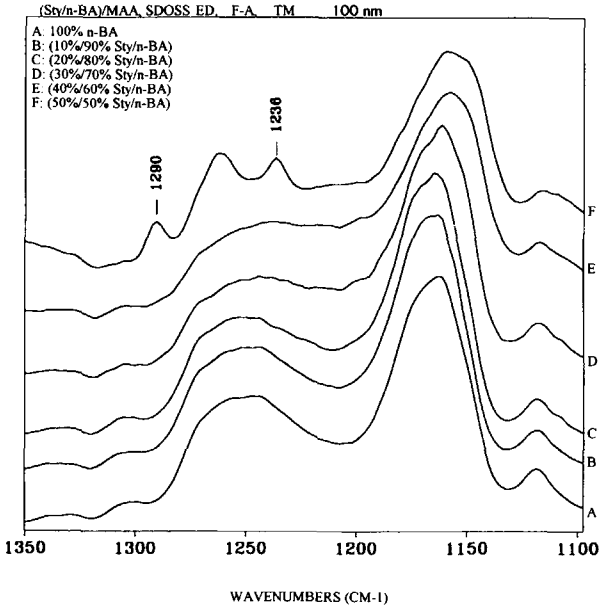

Figure 8 ATR FTIR spectra in the S—O asymmetric stretching region of Sty/*n*-BA latex copolymers with a particle size of 100 nm recorded from the F–A interface with TM polarization: (A) 100% *n*-BA; (B) 10%/90% Sty/*n*-BA; (C) 20%/80% Sty/*n*-BA; (D) 30%/70% Sty/*n*-BA; (E) 40%/60% Sty/*n*-BA; (F) 50%/50% Sty/*n*-BA. (Coalescence time: 6 h).

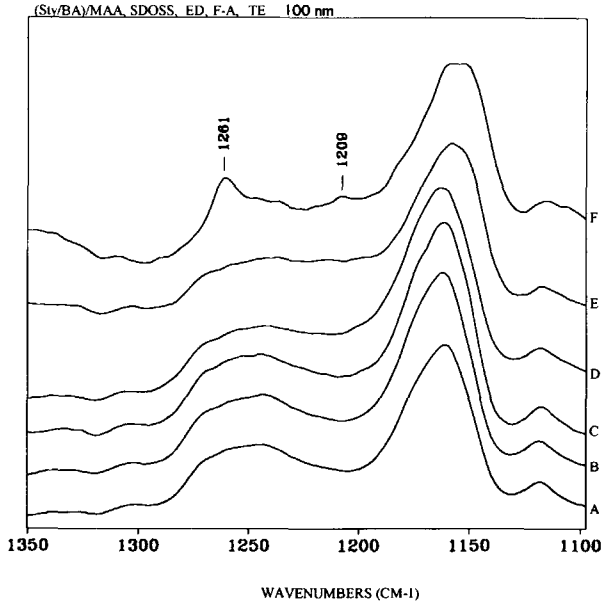

Figure 7 ATR FTIR spectra in the S—O asymmetric stretching region of Sty/*n*-BA latex copolymers with a particle size of 100 nm recorded from the F–A interface with TE polarization: (A) 100% *n*-BA; (B) 10%/90% Sty/*n*-BA; (C) 20%/80% Sty/*n*-BA; (D) 30%/70% Sty/*n*-BA; (E) 40%/60% Sty/*n*-BA; (F) 50%/50% Sty/*n*-BA. (Coalescence time: 6 h).

With this in mind, let us return to the S—O symmetric stretching region and examine the intensity changes resulting from the TE and TM polarizations. As we recall, the bands in the S—O symmetric stretching region at the F–A interface with TE and TM polarizations were shown in Figures 3 and 4, traces (A)–(F), respectively. In Figure 3, the 1056 and 1046 cm^{-1} bands are more pronounced for the 50%/50% Sty/*n*-BA [trace (F)] with TE polarization. In contrast, the spectra of the same specimens recorded with TM polarization show just the opposite behavior. As illustrated in Figure 4, the 1056 cm^{-1} band is much weaker and the intensity of the 1046 cm^{-1} band recorded with the TM polarization (traces A–F) is also diminished. Since the 1056 cm^{-1} band is more pronounced with the TE polarization, the majority of the $SO_3^-Na^+ \cdots HOOC$ associations are preferentially parallel to the latex film surface. This conclusion agrees with the polarization data for the S—O asymmetric stretching bands discussed in the context of the spectra presented in Figures 7 and 8.

Based on the spectroscopic analysis and particle size considerations, the following orientation of $SO_3^-Na^+$ entities can be established, as shown in Figure 9(A). Because the 1046 cm^{-1} band intensities

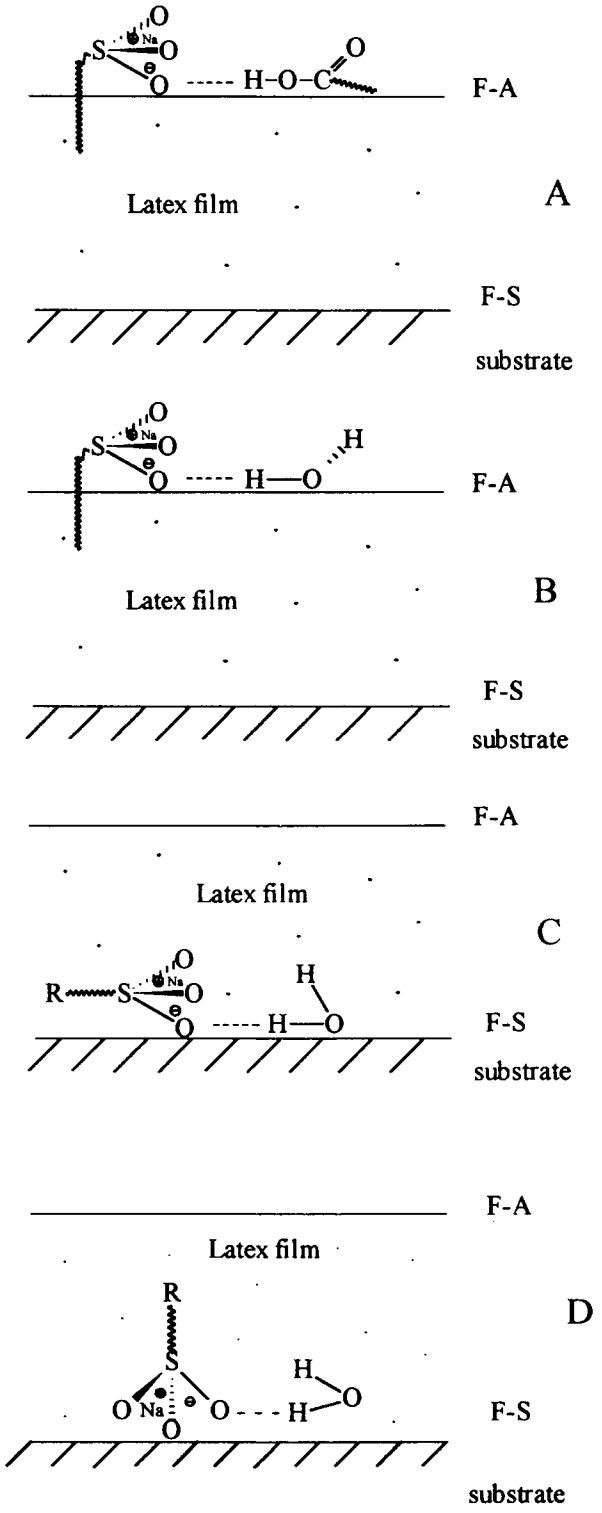

Figure 9 Schematic representation of orientation of SDOSS molecules: (A) $SO_3^-Na^+$ associates with COOH groups at the F–A interface; (B) $SO_3^-Na^+$ associates with H_2O at the F–A interface; (C) SDOSS molecules are parallel to the substrate at the F–S interface; (D) SDOSS molecules are perpendicular to the substrate at the F–S interface.

are stronger in the TE polarization, the majority of the $SO_3^-Na^+ \cdots H_2O$ associations are also preferentially parallel to the film surface, as illustrated in Figure 9(B). On the other hand, the bands at 1290 and 1236 cm^{-1} are not detected with the TE polarization. Because they are more pronounced in the TM polarization [Figs. 7 and 8, trace (F)], the hydrophobic ends on SDOSS are preferentially perpendicular to the latex film surface. However, spectroscopic analysis conducted on the ATR spectra recorded from the F–S interface (not shown) indicated no difference between TE and TM polarizations; therefore, SDOSS molecules exhibit random orientation at this interface. Figure 5A also showed no band at 1056 cm^{-1}, indicating a lack of the $SO_3^-Na^+ \cdots HOOC$ associations at the F–S interface. Based on analysis of these data, molecular arrangements illustrated in Figure 9(C) and (D), are proposed. Hydrophilic $SO_3^-Na^+$ and hydrophobic ends of SDOSS are randomly distributed at the F–S interface. For 100-nm latex particles, preferential orientations of SDOSS molecules at the F–A interface are present, depicted in Figure 9(A) and (B). In contrast, there is no preferential orientation for 50-nm-diameter particles. No preferential orientation at the F–S interface is detected for 100% poly(*n*-BA) latexes with particle sizes of 50 and 100 nm.

Let us return to the particle size effect on surfactant orientation. Based on the analysis of the spectroscopic data, the SDOSS surfactant molecules have a preferential parallel orientation near the F–A interface for larger particle size. One of the several possible factors that may contribute to the surfactant orientation is packing parameter. Assuming uniform distribution of the particles, small particles typically have a higher packing factor and occupy more volume.[17] Therefore, higher packing and the volume occupied by the polymer result in less space for SDOSS surfactant molecules to migrate. In addition, there are fewer H_2O molecules in the latex interstices, resulting in fewer associations of SDOSS with HOOC and H_2O molecules during electrodeposition. In contrast, the larger-particle-size latexes have a small packing factor in comparison with small-particle-size latex, resulting in a large effective space voids between the particles. Therefore, more H_2O molecules exist between the particle interstices, allowing surfactant molecules to migrate and associate with the HOOC and H_2O groups. Thus, a preferential orientation is detected for larger-particle-size latex at the F–A interface.

Another issue that should be addressed is how coalescence is affected by the electrodeposition process. As we have indicated, the electrodeposited films

contain a minimal amount of water. As opposed to a regular latex deposition, where water is an integral part of the deposited film (at least in the early stages), electrodeposited films are dry. However, another effect is associated with the process. Although the films appear to be coalesced, scanning electron microscopy measurements indicate that the particles are in contact, but do not form a continuous phase. As a matter of fact, exposure of electrodeposited films to defined humidity conditions, for example relative humidity (RH) above 30% causes the latex particles to coalesce slowly; the process is accelerated by higher RH.

The above observations, combined with the spectroscopic data for different size latex particles, allow us to identify factors that may influence coalescence process. The factor that influences the surfactant mobility during coalescence is surface tension on the coalescing latex. Because only a small fraction of water is present at the early stages, the particles come into contact with each other, resulting in a close-packed array with water-filled interstices. As a result of contact between two particles, a surface curvature is formed. This is schematically illustrated in Figure 10. Tolman proposed that for such a curvature, the surface tension can be calculated using the following equation[18,19]:

$$\frac{\gamma}{\gamma_0} = \frac{1}{1 + 2\delta/r}$$

where γ is the surface tension of the curvature surface; γ_0 is the surface tension of a latex particle surface; δ is constant; and r is the radius of the curvature surface. From this equation, we can predict that the surface tension decreases as the curvature radius decreases. For 50- and 100-nm latex particles, the estimated radii of the curvature are approximate 12.5 and 22.5 nm, respectively. They are schematically illustrated in Figure 10 (A) and (B). Using these data, the γ/γ_0 ratios for 50- and 100-nm particles are 0.98 and 0.991, respectively.

These results indicate that for a larger particle size, the curvature surface tension that results from a contact between the neighboring particles expels surfactant molecules in order to compensate for the surface tension difference between the contact curvature and the curvature of the latex particles. This is shown in Figure 10(A). On other hand, fewer SDOSS molecules are expelled from smaller-diameter latex particles due to a smaller γ/γ_0 ratio between the two surface tensions. As a result, more surfactant molecules accumulate in the interfacial areas for smaller-particle-size latexes. This is shown in Figure 10(B). It should be kept in mind, however, that the process of expelling SDOSS from the particle interfacial regions is also affected by latex copolymer–surfactant compatibility.

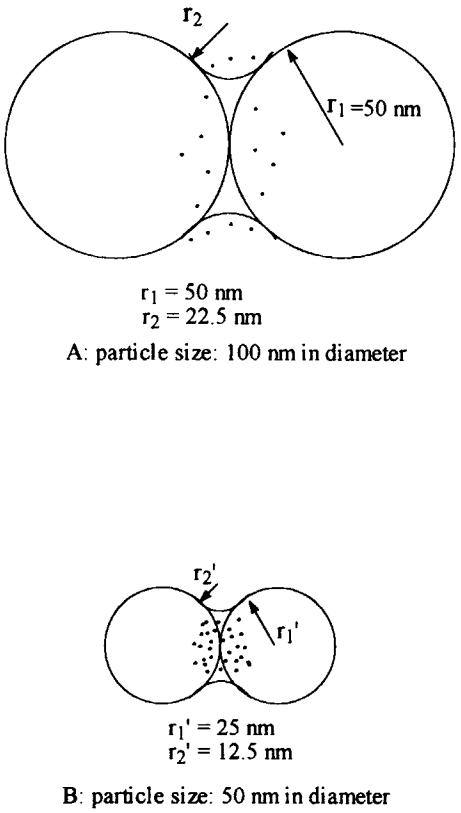

Figure 10 Schematical diagram for the radii on the curvature surface; particle diameter: (A) 100 nm; (B) 50 nm.

CONCLUSIONS

In this study, we introduced a novel means of depositing latex films via electrodeposition. Analysis of spectroscopic data recorded from the F–A and F–S interfaces indicate that the nature of the interactions between surfactant molecules and latex components is affected by the latex particle size and latex particle composition. Analysis of the polarization ATR FTIR results indicates that SDOSS hydrophilic ends will form aggregates with H_2O and COOH latex groups, resulting in parallel or perpendicular interfacial arrays. At the F–A interface, SDOSS hydrophilic ends are preferentially parallel to the surface, and hydrophobic ends are preferentially perpendicular to the surface. In contrast, the hydrophilic $SO_3^-Na^+$ ends have random orientation at the F–S interface.

REFERENCES

1. M. W. Urban and K. W. Evanson, *Polym. Commun.*, **31,** 279 (1990).
2. B.-J. Niu and M. W. Urban, *J. Appl. Polym. Sci.*, **60,** 371 (1996).
3. K. W. Evanson and M. W. Urban, *J. Appl. Polym. Sci.*, **42,** 2287 (1991).
4. K. W. Evanson and M. W. Urban, *J. Appl. Polym. Sci.*, **42,** 2297 (1991).
5. T. A. Thorstenson and M. W. Urban, *J. Appl. Polym. Sci.*, **47,** 1381 (1993).
6. T. A. Thorstenson and M. W. Urban, *J. Appl. Polym. Sci.*, **47,** 1387 (1993).
7. T. A. Thorstenson, L. K. Tebelius, and M. W. Urban, *J. Appl. Polym. Sci.*, **49,** 103 (1993).
8. T. A. Thorstenson and M. W. Urban, *J. Appl. Polym. Sci.*, **50,** 1207 (1993).
9. J. P. W. Kunkel and M. W. Urban, *J. Appl. Polym. Sci.*, **50,** 1217 (1993).
10. B.-J. Niu and M. W. Urban, *J. Appl. Polym. Sci.*, **56,** 377 (1995).
11. J. B. Huang and M. W. Urban, *Appl. Spectrosc.*, **46**(11), 1666 (1992).
12. J. B. Huang and M. W. Urban, *Appl. Spectrosc.*, **47**(7), 973 (1992).
13. B.-J. Niu and M. W. Urban, *J. Appl. Polym. Sci.*, **60,** 389 (1996).
14. J. E. Kluin, H. Moaddel, M. Y. Ruan, Z. Yu, N. M. Jamieson, R. Simha, and J. D. McGervey, in *Structure–Property Relations in Polymers,* M. W. Urban and C. D. Craver, Eds., Advances in Chemistry series 236, American Chemical Society, Washington, DC, 1993, Chap. 20.
15. W. C. Yu, C. S. P. Sung, and R. E. Robertson, *Macromolecules,* **21,** 355 (1988).
16. S. L. Rosen, *Fundamental Principles of Polymeric Materials,* 2nd Ed., John Wiley & Sons, New York, 1993, Chap. 8.
17. Y. Wang, A. Kats, D. Juhue, and M. A. Winnik, *Langmuir,* **8,** 1435 (1992).
18. R. C. Tolman, *J. Chem. Phys.*, **17,** 333 (1949).
19. A. W. Adamson, *Physical Chemistry of Surfaces,* 4th Ed., John Wiley & Sons, New York, 1982, Chap. 3.

Received June 26, 1995
Accepted October 1, 1995